Monthly Notices
of the
ROYAL ASTRONOMICAL SOCIETY

MNRAS **470,** 2723–2735 (2017)
Advance Access publication 2017 May 16

doi:10.1093/mnras/stx1196

Constraining the relative velocity effect using the Baryon Oscillation Spectroscopic Survey

Florian Beutler,[1]★ Uroš Seljak[2,3] and Zvonimir Vlah[4,5]

[1] *Institute of Cosmology and Gravitation, Dennis Sciama Building, University of Portsmouth, Portsmouth PO1 3FX, UK*
[2] *Lawrence Berkeley National Lab, 1 Cyclotron Rd, Berkeley, CA 94720, USA*
[3] *Department of Physics, University of California, Berkeley, CA 94720, USA*
[4] *Stanford Institute for Theoretical Physics and Department of Physics, Stanford University, Stanford, CA 94306, USA*
[5] *Kavli Institute for Particle Astrophysics and Cosmology, SLAC and Stanford University, Menlo Park, CA 94025, USA*

Accepted 2017 May 12. Received 2017 May 11; in original form 2016 December 14

ABSTRACT

We analyse the power spectrum of the Baryon Oscillation Spectroscopic Survey (BOSS) Data Release 12 to constrain the relative velocity effect, which represents a potential systematic for measurements of the baryon acoustic oscillation (BAO) scale. The relative velocity effect is sourced by the different evolution of baryon and cold dark matter perturbations before decoupling. Our power spectrum model includes all one-loop redshift-space terms corresponding to $v_{\rm bc}$ parametrized by the bias parameter b_v^2. We also include the linear terms proportional to the relative density, $\delta_{\rm bc}$, and relative velocity dispersion, $\theta_{\rm bc}$, which we parametrize with the bias parameters $b_\delta^{\rm bc}$ and $b_\theta^{\rm bc}$. Our data does not support a detection of the relative velocity effect in any of these parameters. Combining the low- and high-redshift bins of BOSS, we find limits of $b_{\rm v}^2 = 0.012 \pm 0.015$ (± 0.031), $b_\delta^{\rm bc} = -1.0 \pm 2.5$ (± 6.2) and $b_\theta^{\rm bc} = -114 \pm 55$ (± 175) with 68 per cent (95 per cent) confidence levels. These constraints restrict the potential systematic shift in $D_A(z)$, $H(z)$ and $f\sigma_8$, due to the relative velocity, to 1 per cent, 0.8 per cent and 2 per cent, respectively. Given the current uncertainties on the BAO measurements of BOSS, these shifts correspond to 0.53σ, 0.5σ and 0.22σ for $D_A(z)$, $H(z)$ and $f\sigma_8$, respectively.

Key words: gravitation – surveys – cosmological parameters – dark energy – large-scale structure of Universe – cosmology: observations.

1 INTRODUCTION

Measurements of the baryon acoustic scale in the distribution of galaxies have established themselves as one of the most powerful tools for precision cosmology (Eisenstein, Hu & Tegmark 1998; Percival et al. 2001; Blake & Glazebrook 2003; Hu & Haiman 2003; Linder 2003; Seo & Eisenstein 2003; Cole et al. 2005; Eisenstein et al. 2005; Beutler et al. 2011; Blake et al. 2011; Alam et al. 2016). With the most recent measurements of the BAO scale in the Baryon Oscillation Spectroscopic Survey (BOSS) survey, we have now reached 1 per cent precision in two redshift bins (Alam et al. 2016; Beutler et al. 2016a; Ross et al. 2016).

Given the fact that the baryon acoustic oscillation (BAO) signal is located on very large scales, the impact of any late-time non-linear evolution is small for these measurements, and fairly simple perturbation theory based models can be used to extract the BAO scale (Crocce & Scoccimarro 2008; Padmanabhan, White & Cohn 2009). In the light of the next generation of galaxy redshift surveys like DESI (Schlegel et al. 2009) and *Euclid* (Laureijs et al. 2011), which will reduce the uncertainties on these measurements by another order of magnitude, even small effects to the BAO scale can bias our cosmological constraints.

In this paper, we investigate the relative velocity effect and its impact on anisotropic BAO and Redshift-space distortions (RSD) measurements. The relative velocity effect is sourced by the photon pressure, which prevents baryon perturbations from growing before decoupling. This introduces a relative density $\delta_{\rm bc}$ and velocity divergence $\theta_{\rm bc}$ as well as a relative velocity $v_{\rm bc}$ between cold dark matter (CDM) and baryonic matter. This relative velocity can shift the BAO scale and hence represents a possible systematic for future BAO measurements (Dalal, Pen & Seljak 2010; Yoo & Seljak 2013). The relative velocity effect can impact the BAO scale because it is sourced by the same physical effects that imprinted the BAO scale itself, and hence, this effect acts on the same scale.

The relative velocity $v_{\rm bc}$ is about 30 km s^{-1} at redshift 1000 and decays with $1/a$, reducing it to 0.03 km s^{-1} at redshift zero. Therefore, this effect is negligible at low redshift compared to the far larger virial velocities in galaxy groups and clusters. However, the relative velocity can prevent the condensation of baryons within the

★ E-mail: florian.beutler@port.ac.uk

gravitational potential of the CDM haloes and therefore impact early galaxy formation (Dalal, Pen & Seljak 2010; Tseliakhovich & Hirata 2010; Tseliakhovich, Barkana & Hirata 2011; Naoz, Yoshida & Gnedin 2012; Fialkov et al. 2013). Yoo & Seljak (2013) argue that the modulation of early, low-mass haloes by the relative velocity will effect the subsequent formation of high-mass haloes observed today. Since these processes are not known in detail, the amplitude of the relative velocity effect cannot be predicted and must be constrained by the data.

In this paper, we use the latest BOSS Data Release (DR12) data to constrain the relative velocity effect. While such studies have been done before, there are several novel aspects to our analysis: (1) For the first time, we include the advection term (Blazek, McEwen & Hirata 2015); (2) besides b_v^2, we also set constraints on biasing by the density, $\delta_{\rm bc}$, and velocity divergence, $\theta_{\rm bc}$ (Barkana & Loeb 2011; Schmidt 2016); (3) we include all relative velocity contributions up to one-loop order including the redshift-space terms; and (4) we quantify the potential shifts due to all three relative velocity contributions for the anisotropic BAO and RSD parameters.

This paper is organized as follows: We start with the introduction of the BOSS DR12 data set in Section 2. In Section 3, we present the power spectrum measurements, which we use for our analysis. In Section 4, we discuss the power spectrum model, which is based on perturbation theory and includes the relative velocity terms. In Section 5, we introduce the mock catalogues that we use to test our model. In Section 6, we fit the BOSS measurements and constrain the relative velocity parameters. In Section 7, we quantify the potential systematic uncertainty on the BAO scale, given our constraints on the relative velocity parameters. We further discuss our results in Section 8 before concluding in Section 9.

The fiducial cosmological parameters, which are used to convert the observed angles and redshifts into comoving coordinates and to generate linear power spectrum models as input for the power spectrum templates, follow a flat ΛCDM model with $\Omega_{\rm m} = 0.31$, $\Omega_{\rm b}h^2 = 0.022$, $h = 0.676$, $\sigma_8 = 0.824$, $n_{\rm s} = 0.96$, $\sum m_\nu = 0.06\,{\rm eV}$ and $r_{\rm s}^{\rm fid} = 147.78$ Mpc. These parameters are the fiducial cosmological parameters used for the BOSS DR12 data analysis and are close to the Planck 2015 cosmological constraints within ΛCDM.

2 THE BOSS DR12 DATA SET

BOSS, as part of SDSS-III (Eisenstein et al. 2011; Dawson et al. 2012), measured spectroscopic redshifts of 1198 006 galaxies making use of the SDSS multifibre spectrographs (Bolton et al. 2012; Smee et al. 2013). The galaxies are selected from multicolour SDSS imaging (Fukugita et al. 1996; Gunn et al. 1998; Smith et al. 2002; Gunn et al. 2006; Doi et al. 2010) over 10 252 deg^2 divided in two patches on the sky and cover a redshift range of $z = 0.2$–0.75. The final BOSS DR12 analysis splits this redshift range in three overlapping redshift bins defined by $0.2 < z < 0.5$, $0.4 < z < 0.6$ and $0.5 < z < 0.75$ with the effective redshifts $z_{\rm eff} = 0.38$, 0.51 and 0.61. In this analysis, we will ignore the middle redshift bin, since it is highly correlated with the other two redshift bins and does not add much additional information.

We include three different incompleteness weights to account for shortcomings of the BOSS data set (see Ross et al. 2012; Anderson et al. 2014 for details): a redshift failure weight, $w_{\rm rf}$, a fibre collision weight, $w_{\rm fc}$, and a systematics weight, $w_{\rm sys}$, which is a combination of a stellar density weight and a seeing condition weight. Each galaxy is thus counted as

$$w_{\rm c} = (w_{\rm rf} + w_{\rm fc} - 1)w_{\rm sys}. \tag{1}$$

More details about these weights and their effect on the DR12 sample can be found in Ross et al. (2016).

3 BOSS MEASUREMENTS AND UNCERTAINTIES

The power spectrum measurements used in this paper make use of the FFT-based estimator (Bianchi et al. 2015; Scoccimarro 2015) and are discussed in more detail in Beutler et al. (2016a,b). Here, we will summarize these measurements but refer to the above mentioned references for more details.

The first three non-zero power spectrum multipoles can be calculated as (Feldman, Kaiser & Peacock 1994)

$$P_0(\boldsymbol{k}) = \frac{1}{2A}[F_0(\boldsymbol{k})F_0^*(\boldsymbol{k}) - S], \tag{2}$$

$$P_2(\boldsymbol{k}) = \frac{5}{4A}F_0(\boldsymbol{k})[3F_2^*(\boldsymbol{k}) - F_0^*(\boldsymbol{k})], \tag{3}$$

$$P_4(\boldsymbol{k}) = \frac{9}{16A}F_0(\boldsymbol{k})\left[35F_4^*(\boldsymbol{k}) - 30F_2^*(\boldsymbol{k}) + F_0^*(\boldsymbol{k})\right], \tag{4}$$

where the shot noise and the normalization are given by

$$S = (1+\alpha)\int {\rm d}^3x n_{\rm g}(x) w_{\rm FKP}^2(x), \tag{5}$$

$$A = \int {\rm d}^3x n_{\rm g}(x) w_{\rm FKP}(x), \tag{6}$$

with α being the ratio between the number of galaxies and randoms. The Fourier-space density moments are given by

$$F_0(\boldsymbol{k}) = A_0(\boldsymbol{k}), \tag{7}$$

$$F_2(\boldsymbol{k}) = \frac{1}{k^2}\left[k_x^2 B_{xx} + k_y^2 B_{yy} + k_z^2 B_{zz} + 2(k_x k_y B_{xy} + k_x k_z B_{xz} + k_y k_z B_{yz})\right], \tag{8}$$

$$\begin{aligned} F_4(\boldsymbol{k}) = \frac{1}{k^4}\Big[&k_x^4 C_{xxx} + k_y^4 C_{yyy} + k_z^4 C_{zzz} \\ &+ 4\left(k_x^3 k_y C_{xxy} + k_x^3 k_z C_{xxz} + k_y^3 k_x C_{yyx}\right. \\ &\left. + k_y^3 k_z C_{yyz} + k_z^3 k_x C_{zzx} + k_z^3 k_y C_{zzy}\right) \\ &+ 6\left(k_x^2 k_y^2 C_{xyy} + k_x^2 k_z^2 C_{xzz} + k_y^2 k_z^2 C_{yzz}\right) \\ &+ 12 k_x k_y k_z (k_x C_{xyz} + k_y C_{yxz} + k_z C_{zxy})\Big]. \end{aligned} \tag{9}$$

Following Bianchi et al. (2015) and Scoccimarro (2015), we can write

$$A_0(\boldsymbol{k}) = \int {\rm d}\boldsymbol{r}\, D(\boldsymbol{r}) {\rm e}^{i\boldsymbol{k}\cdot\boldsymbol{r}}, \tag{10}$$

$$B_{xy}(\boldsymbol{k}) = \int {\rm d}\boldsymbol{r} \frac{r_x r_y}{|\boldsymbol{r}|^2} D(\boldsymbol{r}) {\rm e}^{i\boldsymbol{k}\cdot\boldsymbol{r}}, \tag{11}$$

$$C_{xyz}(\boldsymbol{k}) = \int {\rm d}\boldsymbol{r} \frac{r_x^2 r_y r_z}{|\boldsymbol{r}|^4} D(\boldsymbol{r}) {\rm e}^{i\boldsymbol{k}\cdot\boldsymbol{r}}, \tag{12}$$

where $D(\boldsymbol{r})$ is the galaxy overdensity field. The three equation above can be calculated using FFTs.

3.1 Covariance matrix

To derive a covariance matrix for the power spectrum multipoles, we use 2048[1] MultiDark-Patchy mock catalogues (Kitaura et al. 2016). These mock catalogues have been calibrated to an N-body-based reference sample using approximate gravity solvers and analytical–statistical biasing models. The reference catalogue is extracted from one of the BigMultiDark simulations (Klypin et al. 2014), which used 3840^3 particles on a volume of $(2.5\,h^{-1}\ \mathrm{Gpc})^3$ assuming a ΛCDM cosmology with $\Omega_\mathrm{M} = 0.307\,115$, $\Omega_\mathrm{b} = 0.048\,206$, $\sigma_8 = 0.8288$, $n_\mathrm{s} = 0.9611$, and a Hubble constant of $H_0 = 67.77\ \mathrm{km\ s^{-1}\ Mpc^{-1}}$.

3.2 Window function

Before comparing any model to the power spectrum measurement, we convolve it with the survey window function using the technique discussed in section 4 of Beutler et al. (2016b), which is based on Wilson et al. (2015). The technique applies the following steps to turn a power spectrum model without any window function effect into the required convolved power spectrum including the survey window function:

(i) Calculate the model power spectrum multipoles and Fourier-transform them to obtain the correlation function multipoles $\xi_L^\mathrm{model}(s)$.

(ii) Calculate the 'convolved' correlation function multipoles $\hat{\xi}_\ell^\mathrm{model}(s)$ by multiplying the correlation function with the window function multipoles.

(iii) Conduct 1D FFTs to transform the convolved correlation function multipoles back into Fourier space to obtain the convolved power spectrum multipoles, $\hat{P}_\ell^\mathrm{model}(k)$. This result becomes our model to be compared with the observed power spectrum multipoles.

For more details about the implementation, we refer to Beutler et al. (2016b).

4 POWER SPECTRUM MODEL

The power spectrum model we employ in this paper is an extension of the model used in Beutler et al. (2014, 2016b) and builds upon the work of Taruya, Nishimichi & Saito (2010a), McDonald & Roy (2009a) and Saito et al. (2014a). Here, we extend this model by including the relative velocity terms following the approach of Yoo, Dalal & Seljak (2011) and Blazek et al. (2015) with the addition of redshift-space distortion terms, which describe the couplings of the density field with the velocity divergence field. We also include the linear terms $P_{\delta|\delta_\mathrm{bc}}(k)$ and $P_{\delta|\theta_\mathrm{bc}}(k)$ as discussed in Schmidt (2016).

We define the galaxy density field as

$$\begin{aligned}\delta_\mathrm{g}^s(x) = {} & b_1\delta_\mathrm{m}(x) + \frac{1}{2}b_2\left[\delta_\mathrm{m}^2(x) - \langle\delta_\mathrm{m}^2\rangle\right] + \frac{1}{2}b_s\left[s^2(x) - \langle s^2\rangle\right] + \ldots \\ & + b_\mathrm{v}^2\left[\mathrm{v}_\mathrm{bc}^2(x) - \langle v_\mathrm{bc}^2\rangle\right] \\ & + b_\delta^\mathrm{bc}\left[\delta_\mathrm{b}(x) - \delta_c(x)\right] + b_\theta^\mathrm{bc}\left[\theta_\mathrm{b}(x) - \theta_\mathrm{c}(x)\right] + \ldots,\end{aligned} \tag{13}$$

where $\delta_\mathrm{m}(x)$ is the matter density field, $v_\mathrm{bc}(x)$ is the relative velocity field, $s(x)$ is the tidal tensor field, $\delta_\mathrm{bc}(x)$ is the relative density field between baryons and CDM, and $\theta_\mathrm{bc}(x)$ is the relative velocity divergence field. The power spectrum for the density field above is

$$\begin{aligned}P_\mathrm{g}(k,\mu) = {} & P_\mathrm{g,NL}(k,\mu) + b_\mathrm{v}^2\left[b_1 P_{\delta|\mathrm{v}^2}(k) + b_2 P_{\delta^2|\mathrm{v}^2}(k)\right. \\ & \left. + b_s P_{s^2|\mathrm{v}^2}(k) + b_\mathrm{v}^2 P_{\mathrm{v}^2|\mathrm{v}^2}(k)\right] \\ & + b_1 b_\mathrm{v}^2 P_{\mathrm{adv}|\delta}(k) + 2b_1 b_\delta^\mathrm{bc} P_{\delta|\delta_\mathrm{bc}} + 2b_1 b_\theta^\mathrm{bc} P_{\delta|\theta_\mathrm{bc}} \\ & - 2f\mu^2\left[b_\mathrm{v}^2\left(b_1 P_{\delta|\mathrm{v}^2\mathrm{v}_\parallel}(k) + P_{\mathrm{adv}|\mathrm{v}_\parallel}(k)\right)\right. \\ & \left. - b_\theta^\mathrm{bc} P_{\delta|\theta_\mathrm{bc}} + b_\delta^\mathrm{bc} P_{\delta|\delta_\mathrm{bc}} + b_\mathrm{v}^2\left(P_{\mathrm{v}^2|\mathrm{v}_\parallel}(k) + P_{\mathrm{v}^2|\delta\mathrm{v}_\parallel}(k)\right)\right] \\ & + f^2\mu^4 b_\mathrm{v}^2 P_{\mathrm{v}_\parallel|\mathrm{v}^2\mathrm{v}_\parallel}(k) - f^2\mu^2 b_\mathrm{v}^2\left[I_1(k) + \mu^2 I_2(k)\right],\end{aligned} \tag{14}$$

where we ignored the $b_\theta^{\mathrm{bc},2}$ and $b_\delta^{\mathrm{bc},2}$ terms, which, in our case, are expected to be about one order of magnitude smaller compared to the linear terms (Schmidt 2016). All the different terms in the equation above are defined in Appendix A. The first term, $P_\mathrm{g,NL}$, describes the linear and non-linear terms connecting the real-space matter density field with the redshift-space galaxy density field, and is given by

$$\begin{aligned}P_\mathrm{g,NL}(k,\mu) = {} & \exp\left\{-(fk\mu\sigma_\mathrm{v})^2\right\}\left[P_{\mathrm{g},\delta\delta}(k) + 2f\mu^2 P_{\mathrm{g},\delta\theta}(k)\right. \\ & + f^2\mu^4 P_{\theta\theta}(k) \\ & \left. + b_1^3 A(k,\mu,\beta) + b_1^4 B(k,\mu,\beta)\right],\end{aligned} \tag{15}$$

with

$$\begin{aligned}P_{\mathrm{g},\delta\delta}(k) = {} & b_1^2 P_{\delta\delta}(k) + b_2 b_1 P_{\mathrm{b}2,\delta}(k) + b_{s2} b_1 P_{\mathrm{b}s2,\delta}(k) \\ & + 2b_{3\mathrm{nl}} b_1 \sigma_3^2(k) P_\mathrm{m}^\mathrm{lin}(k) + b_2^2 P_{\mathrm{b}22}(k) \\ & + b_2 b_{s2} P_{b2s2}(k) + b_{s2}^2 P_{\mathrm{b}s22}(k) + N,\end{aligned} \tag{16}$$

$$\begin{aligned}P_{\mathrm{g},\delta\theta}(k) = {} & b_1 P_{\delta\theta}(k) + b_2 P_{\mathrm{b}2,\theta}(k) + b_{s2} P_{\mathrm{b}s2,\theta}(k) \\ & + b_{3\mathrm{nl}}\sigma_3^2(k) P_\mathrm{m}^\mathrm{lin}(k).\end{aligned} \tag{17}$$

The terms A and B in equation (15) account for coupling between the density field and the velocity field (Taruya, Nishimichi & Saito 2010b), σ_v is a free parameter describing the velocity dispersion on quasi-linear scales and N is another free parameter used to marginalize over any constant non-Poisson shot noise. This is the base redshift-space model of McDonald & Roy (2009b), Taruya et al. (2010b) and Saito et al. (2014b), which has been tested extensively in Beutler et al. (2014, 2016b). In this paper, we focus on the relative velocity extensions to this model. The dominant terms in equation (14), with respect to the relative velocity effects, are

$$P_{\mathrm{adv}|\delta}(k) = \frac{4}{3}T_\mathrm{v}(k) k P_\mathrm{lin}(k)\int\frac{k\,\mathrm{d}k}{2\pi^2}T_\mathrm{v}(k)P_\mathrm{lin}(k), \tag{18}$$

$$P_{\delta|\mathrm{v}^2}(k) = 4\int\frac{\mathrm{d}^3\boldsymbol{q}}{(2\pi)^3}P_\mathrm{m}^\mathrm{lin}(q)P_\mathrm{m}^\mathrm{lin}(k-q) \tag{19}$$

$$\times\, F_2(\boldsymbol{q},\boldsymbol{k}-\boldsymbol{q})G_u(\boldsymbol{q},\boldsymbol{k}-\boldsymbol{q})\frac{\boldsymbol{q}\cdot(\boldsymbol{k}-\boldsymbol{q})}{\boldsymbol{q}(\boldsymbol{k}-\boldsymbol{q})}, \tag{20}$$

$$P_{\delta|\delta_\mathrm{bc}}(k) = T_\mathrm{bc}(k)P_\mathrm{lin}(k), \tag{21}$$

$$P_{\delta|\theta_\mathrm{bc}}(k) = \frac{\sigma_\mathrm{vbc}}{H_0}T_\mathrm{v}(k)k P_\mathrm{lin}(k), \tag{22}$$

[1] To be precise, we have 2048 mocks for the SGC and 2045 mocks for the NGC.

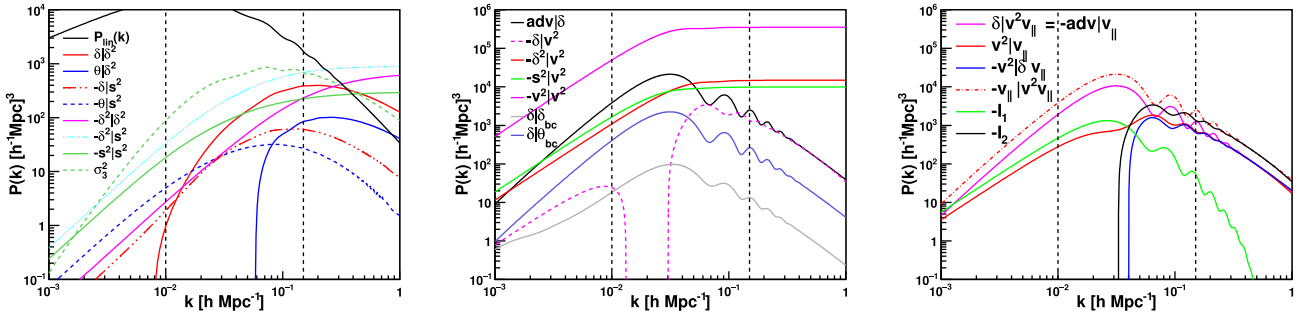

Figure 1. Comparison of the different perturbative terms used in our power spectrum model (see equation 14 and Appendix A). Left-hand panel: comparison of the density and velocity terms; middle panel: comparison of the correlations between the density field and the relative velocity field; right-hand panel: correlation between the relative velocity field and the velocities. The fitting results presented in this paper make use of the scales between the two dashed lines.

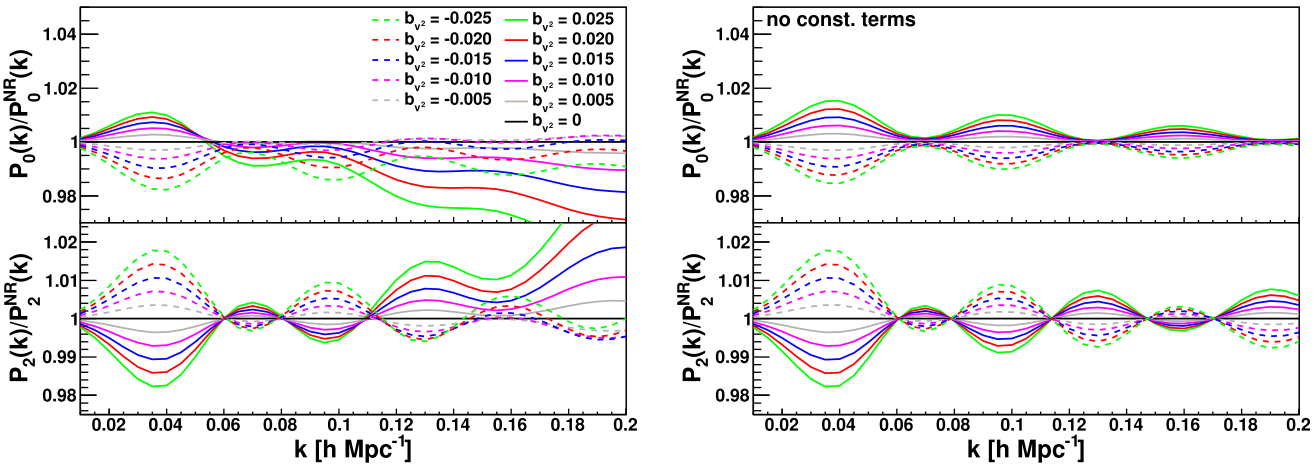

Figure 2. This plot shows the effect of the b_v^2 parameter to the power spectrum monopole (top panel) and quadrupole (bottom panel). $P_\ell^{\rm NR}(k)$ is the power spectrum multipole with all relative velocity parameters set to zero. All other parameters are fixed. The plot on the right-hand side excludes the terms $P_{v^2v^2}$, $P_{\delta^2v^2}$ and $P_{s^2v^2}$, in which case b_v^2 does not have any effect on the amplitude but purely changes the oscillation pattern.

with the kernels

$$F_2(\boldsymbol{k}_1,\boldsymbol{k}_2) = \frac{5}{7} + \frac{\boldsymbol{k}_1\cdot\boldsymbol{k}_2}{2}\left(\frac{1}{k_1^2}+\frac{1}{k_2^2}\right) + \frac{2}{7}\left(\frac{\boldsymbol{k}_1\cdot\boldsymbol{k}_2}{k_1k_2}\right)^2, \tag{23}$$

$$G_u(\boldsymbol{k}_1,\boldsymbol{k}_2) = -T_{\rm v}(k_1)T_{\rm v}(k_2) \tag{24}$$

and the velocity transfer function

$$T_{\rm v}(k) \propto \frac{T_{v_{\rm b}}(k) - T_{\rm v,cdm}(k)}{T_{\rm m}(k)}, \tag{25}$$

where $T_{v_{\rm b}}$ and $T_{\rm v,cdm}$ are the velocity transfer functions of baryons and CDM, respectively. The matter transfer function equivalent is defined as

$$T_{\rm bc}(k) = \frac{T_{\rm b}(k) - T_{\rm cdm}(k)}{T_{\rm m}(k)}. \tag{26}$$

The normalization for the velocity transfer function is given by the square root of

$$\sigma_{\rm vbc}^2 = \int \frac{k^2\,{\rm d}k}{2\pi^2} T_{\rm v}^2(k) P_{\rm lin}(k), \tag{27}$$

which is dimensionless, since $T_{\rm v}$ defined in equation (25) is dimensionless. Note that the advection term and the relative velocity divergence term are related by $P_{{\rm adv}|\delta}(k) = A P_{\delta|\theta_{\rm bc}}(k)$, with

$$A = \frac{4H_0}{3\sigma_{\rm vbc}} \int \frac{k{\rm d}k}{2\pi^2} T_{\rm v}(k) P(k), \tag{28}$$

where we use $H_0^{-1} = 2997\,{\rm Mpc}$ and $\sigma_{\rm vbc} = 1.64\times10^{-6}$, resulting in $A = 1820$ at $z = 0.38$ and $A = 2044$ at $z = 0.61$. While $P_{\delta|\delta_{\rm bc}}(k)$ constrains the bias parameter $b_\delta^{\rm bc}$ and $P_{\delta|\theta_{\rm bc}}(k)$ constrains $b_\theta^{\rm bc}$, the relative velocity bias b_v^2 is constrained by the sum of $P_{{\rm adv}|\delta}(k)$ and $P_{\delta|{\rm v}^2}(k)$.

We follow the nomenclature of Blazek et al. (2015), meaning that our velocity bias $b_{\rm v}^2$ is a factor of 3 times smaller compared to Yoo & Seljak (2013). A list of all terms in equation (14) is given in Appendix A and included in Fig. 1. The figure clearly highlights the oscillations present in some of the relative velocity terms. These oscillations are the main reason for our study, since these oscillations are out of phase with the BAOs and therefore represent a potential bias when measuring the BAO scale.

In our fits, we do not vary b_s and $b_{\rm 3nl}$ freely, but fix them to

$$b_s = -\frac{4}{7}(b_1 - 1), \tag{29}$$

$$b_{\rm 3nl} = \frac{32}{315}(b_1 - 1), \tag{30}$$

which is in good agreement with what is observed in simulations (Saito et al. 2014a) and can be motivated from theory (Baldauf, Seljak & Desjacques 2012; Chan, Scoccimarro & Sheth 2012; Saito et al. 2014b). See also Desjacques, Jeong & Schmidt 2016 for a recent review on large-scale galaxy bias.

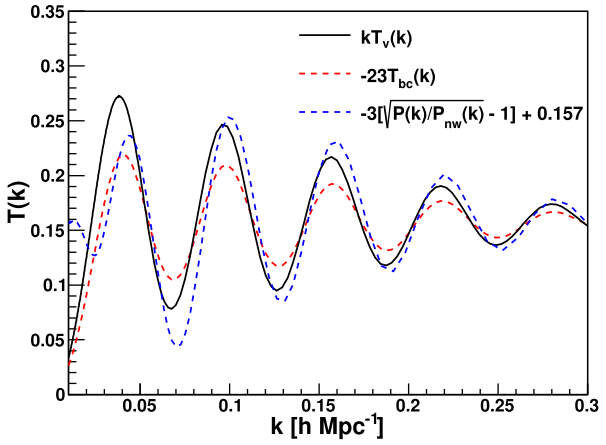

Figure 3. This plot compares the BAO signature in the transfer function $T_{\rm v}$, which is underlying the advection term $P_{\delta|\theta_{\rm bc}}$, and $T_{\rm bc}$, which underlies the term $P_{\delta|\delta_{\rm bc}}$. We also include the $P/P_{\rm nw}$ term, which describes the linear BAO. The $P/P_{\rm nw}(k)$ and $T_{\rm bc}$ terms are scaled to put all functions on the same scale. The different phases of these oscillations are the reason why the relative velocity effect is a potential systematic for BAO measurements.

4.1 Discussion of the power spectrum model

The relative velocity density field $\delta_{\rm bc}$ describes the variation in the CDM-to-baryon ratio, given the fact that baryons and CDM start off with different initial conditions after decoupling. The relative velocity divergence $\theta_{\rm bc}$ captures the same effect in the velocity field. The term $P_{\delta|\delta_{\rm bc}}(k)$ corresponds to correlations between variations of the baryon-to-CDM ratio and the overall matter density field, and $P_{\delta|\theta_{\rm bc}}(k)$ corresponds to correlations of the relative velocity divergence fields with the overall matter density field. While the first term is expected to be of the order of 1, the second term is expected to be of the order of $\approx 6.8[(1+z)H_0]^{-1}(b_1-1)$ (Schmidt 2016). All terms that are proportional to $b_{\rm v}^2$ decay with redshift ($\propto 1/a$).

Our power spectrum model uses the CLASS (Lesgourgues 2011) transfer function output to calculate the velocity transfer function in equation (25). At high redshift, the relative velocity transfer function evolves with the scalefactor, which does not enter our calculation, since this scaling is removed by our normalization in equation (27). Since we assume that all imprints of the relative velocity effects come from $z > 15$, we use the $z = 15$ transfer function and ignore any low-redshift effects.

5 TEST ON MOCK CATALOGUES

We first test our power spectrum model on N-body simulations before using the BOSS Mutidark-Patchy mock catalogues.

5.1 Test on N-body simulations

To test our fitting technique, we use two different sets of N-body simulations, designated as runA and runPB. The runA simulations are 20 halo catalogues of size $[1500\ h^{-1}\,{\rm Mpc}]^3$ with 1500^3 particles using the fiducial cosmology of $\Omega_{\rm m} = 0.274$, $\Omega_\Lambda = 0.726$, $n_{\rm s} = 0.95$, $\Omega_{\rm b} = 0.0457$, $H_0 = 70\,{\rm km\ s^{-1}\ Mpc^{-1}}$ $f\sigma_8(z = 0.55) = 0.455$ and $r_{\rm s}(z_{\rm d}) = 104.503\ h^{-1}\,{\rm Mpc}$. The runPB simulations are 10 galaxy catalogues of size $[1380\ h^{-1}\,{\rm Mpc}]^3$ with $\Omega_{\rm m} = 0.292$, $\Omega_\Lambda = 0.708$, $n_{\rm s} = 0.965$, $\Omega_{\rm b} = 0.0462$, $H_0 = 69\,{\rm km\ s^{-1}\ Mpc^{-1}}$, $f\sigma_8(z = 0.55) = 0.472$ and $r_{\rm s}(z_{\rm d}) = 102.3477\ h^{-1}\,{\rm Mpc}$. The runPB simulations make use of a CMASS-like halo occupation distribution model to populate dark matter haloes with galaxies (see Reid et al. 2014 for details). The fundamental modes for these simulations are $2\pi/[1500\,{\rm Mpc}\,h^{-1}] = 0.0042\,h\ {\rm Mpc}^{-1}$ for runA and $2\pi/[1380\,{\rm Mpc}\,h^{-1}] = 0.0046\,h\ {\rm Mpc}^{-1}$ for runPB, which is below the $k_{\rm min} = 0.01\,h\ {\rm Mpc}^{-1}$ used in our fits.

We measure the power spectrum monopole, quadrupole and hexadecapole, and fit these measurements with the model discussed in the last section. Given that we are working with periodic boxes, we can ignore window function effects for now. The results are summarized in Tables B1 and B2. For these tests, we fix the cosmological parameters ($\alpha_\parallel$, $\alpha_\perp$ and $f\sigma_8$) to their fiducial values.

5.2 Fits to runA simulations

A table summarizing the fitting results for the runA simulations is included in the appendices (Table B1). When varying the individual relative velocity parameters, we see significant biases (at the level of 3σ) in all three relative velocity parameters, while there are no biases if $b_{\rm v}^2$ and b_δ are varied simultaneously. However, degeneracies between the parameters increase the uncertainties by factors of 3 and 1.3 for $b_{\rm v}^2$ and $b_\delta^{\rm bc}$, respectively, compared to the fits where each relative velocity parameter is varied individually.

In Fig. 4, we compare the best-fitting models with and without $b_{\rm v}^2$ and $b_\delta^{\rm bc}$. While the bias in both parameters is only on the 3σ level, it seems to be driven by small scales.

5.3 Fits to runPB simulations

A table summarizing the fitting results for the runPB simulations is included in the appnedices (Table B2). The fits to runPB are consistent with what we saw for the runA simulations, even though the significance of the detected bias in the relative velocity terms is now $<2\sigma$ due to the larger uncertainties in the runPB mocks.

5.4 Tests on the Multidark-Patchy mock catalogues

In Tables B3 and B4, we included the results when fitting the mean of the Multidark-Patchy power spectra for the high- and low-redshift bins. These fits now include the window function treatment described in Section 3.2. The results are consistent with the runA and runPB simulations, meaning that we detect a shift in all three relative velocity parameters.

5.5 Summary: model tests with simulations

We summarized the results for the three different bias parameters from the three mock catalogues in Table 1.

Given that none of our mock catalogues includes the relative velocity effect, we expect all relative velocity parameters to be consistent with zero. However, we detected shifts in the relative velocity parameters, which are consistent in all three sets of mock catalogues. We investigated these biases further by (1) only using the monopole, (2) replacing the Multidark-Patchy covariance matrix with a linear Gaussian covariance matrix, (3) using the real-space power spectrum instead of the one in redshift space, (4) varying b_{s^2} and $b_{\rm 3nl}$ freely instead of fixing them by the relations in equation (30), and (5) introducing the leading scale-dependent bias term $2b_1R^2k^2P_{\rm lin}(k)$ to equation 16 (Okumura et al. 2015). None of these changes to the model was able to explain the biases we measure. We therefore conclude that these biases represent a shortcoming of our model.

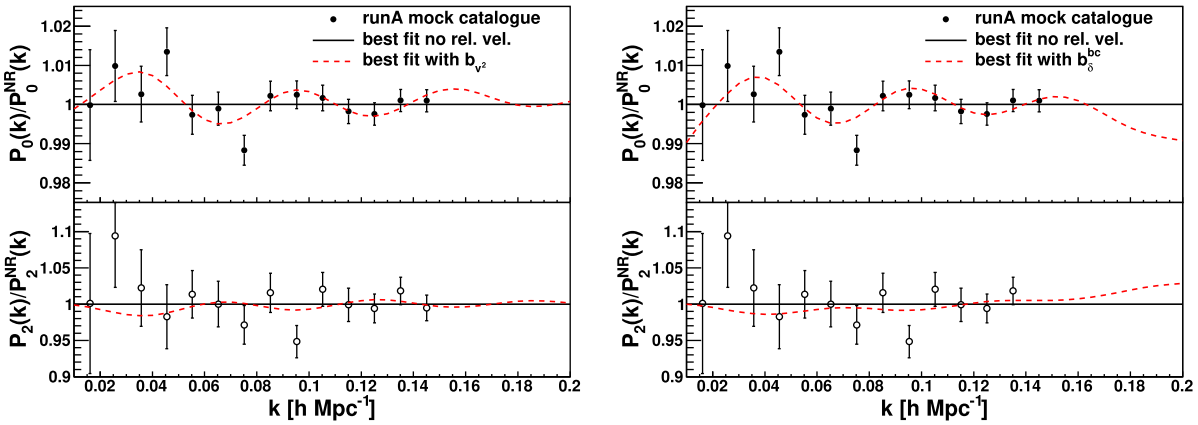

Figure 4. These plots compare the best fitting model for the runA simulations setting all relative velocity parameters to zero (black line) with the fit including b_v^2 (left-hand panel, red dashed line) and b_δ^{bc} (right-hand panel, red dashed line). $P^{NR}(k)$ refers to the power spectrum model with all relative velocity parameters set to zero. The solid points show the mean monopole measurements for the 20 runA simulations and the open points show the equivalent for the quadrupole. The $\Delta\chi^2$ between the solid black line and the red dashed line is $20.9 - 16.2 = 4.7$ for b_v^2 and $20.9 - 15.9 = 5.0$ for b_δ^{bc}. This means that we have a moderate 2.2σ significance for a non-zero value for these bias parameters, even though these values are expected to be zero, given that the simulations do not include a relative velocity effect.

Table 1. This table shows the fitting results to the runA, runPB and the Multidark-Patchy mock catalogues including the relative velocity parameters b_v^2, b_δ^{bc} and b_θ^{bc}. For these tests we fix the parameters $\alpha_\perp$, $\alpha_\parallel$ and $f\sigma_8$ to their fiducial values. Note that these tests have been done for each parameter separately. meaning that the constraints on b_v^2 assume $b_\delta^{bc} = b_\theta^{bc} = 0$, etc. The errors refer to the 1σ and 2σ (in parentheses) uncertainties. All simulations show consistent results for the three bias parameters, including a systematic shift, which we take into account when fitting the data (see Section 6).

	Only b_v^2 (runA)		Only b_v^2 (runPB)		Only b_v^2 (patchy z_1)		Only b_v^2 (patchy z_3)	
	max. like.	mean	max. like.	mean	max. like.	mean	max. like.	mean
$\alpha_\perp$	1	1	1	1	1	1	1	1
$\alpha_\parallel$	1	1	1	1	1	1	1	1
$f\sigma_8$	0.455	0.455	0.472	0.472	0.484	0.484	0.478	0.478
$b_v^2[10^{-3}]$	21.9	$22.2 \pm 6.8(\pm 14)$	19	$20 \pm 11(\pm 21)$	29.1	$29.8 \pm 5.0(\pm 9.6)$	27.6	$27.0^{+6.2}_{-7.9}(^{+19}_{-22})$
b_δ^{bc}	−3.6	$-3.5 \pm 1.1(\pm 2.1)$	−2.2	$-2.3 \pm 1.5(\pm 3.0)$	−4.96	$-4.78 \pm 0.78(\pm 1.6)$	−3.44	$-3.47 \pm 0.66(\pm 1.3)$
b_θ^{bc}	142	$147 \pm 51(^{+170}_{-98})$	82	$77 \pm 63(\pm 120)$	187.2	$187.0 \pm 6.8(\pm 9.6)$	191.9	$192.5 \pm 6.5(\pm 9.4)$

The detected shifts are of the order of 1σ when compared to the measurement uncertainties on these parameters we report in Section 6. Therefore, they are not negligible and need to be taken into account when analysing the BOSS power spectrum.

Using the fitting results of Table 1, we can quantify the systematic shifts in the parameters of interest. The uncertainty-weighted mean for all three simulations is $b_v^2 = 0.0265 \pm 0.0033$, $b_\delta^{bc} = -3.79 \pm 0.44$ and $b_\theta^{bc} = 187.2 \pm 4.7$.

For the case where we have b_v^2 and b_δ^{bc} as free parameters, we also have to account for their correlation. We found mean shifts from the truth of 0.036 in b_v^2 and 1.5 in b_δ^{bc}. The correlation between these two values is 77 per cent and the covariance matrix is

$$C = \begin{pmatrix} 0.033 & 3.629 \\ 3.629 & 676.6 \end{pmatrix} \times 10^{-3}, \quad (31)$$

where the top left-hand corner corresponds to the b_v^2 autocorrelation and the bottom right-hand corner corresponds to the b_δ^{bc} autocorrelation. When fitting the data, we correct the best-fitting values by these systematic shifts and include the error on these values in the error budget.

6 BOSS DR12 ANALYSIS

We are now fitting the power spectrum multipoles using the model of Section 4 including the relative velocity terms. Schmidt (2016) suggests that the dominant relative velocity contribution is given by b_δ^{bc} followed by b_v^2, while the contribution by b_θ^{bc} should be quite small. We fit each relative velocity parameter in turn but also consider the two parameter extension with the two dominant terms b_δ^{bc} and b_v^2. Our fits include the monopole and quadrupole in the range $0.01 < k < 0.15\,h^{-1}$ Mpc and the hexadecapole with $0.01 < k < 0.10\,h^{-1}$ Mpc. The systematic uncertainties on the relative velocity parameters have been quantified in Section 5 and we will correct our best-fitting values by the observed systematic shift. We also include the error on the systematic shift in our error budget. We note that the systematic shifts we found in our tests on mock catalogues are $<2\sigma$ of the BOSS measurement uncertainties and the error on the systematic shift is not contributing significantly to our error budget.

As discussed in Beutler et al. (2016b), we use separate nuisance parameters for the NGC and SGC, given small differences in their selection, which affect the bias parameters. We ignored the middle redshift bin of BOSS DR12, which has been used in other studies of this data set, since it is strongly correlated with the other two redshift bins and does not provide much additional information.

We summarize our fitting results for the two redshift bins and the three relative velocity parameters in Tables 2 and 3. The BOSS DR12 data does not support a detection of any of the three relative velocity parameters. The reduced χ^2 for

Table 2. Fits to the BOSS DR12 combined sample power spectrum multipoles in the low-redshift bin $0.2 < z < 0.5$. The fit includes the monopole and quadrupole in the range $0.01 < k < 0.15\,h^{-1}$ Mpc and the hexadecapole in the range $0.01 < k < 0.10\,h^{-1}$ Mpc. All errors in this table are the marginalized 68 per cent confidence levels, except for the error on the relative velocity parameters b_v^2, b_δ^{bc} and b_θ^{bc}, where we show both the 68 per cent and 95 per cent confidence levels. We show fits including each relative velocity parameter in turn, meaning that columns 2 and 3 show the fits with b_v^2 as a free parameter, assuming $b_\delta^{bc} = b_\theta^{bc} = 0$, etc. The relative velocity parameters are corrected by the bias we detected in the mock catalogues ($b_v^2 = 0.0265 \pm 0.0033$, $b_\delta^{bc} = -3.79 \pm 0.44$ and $b_\theta^{bc} = 187.2 \pm 4.7$, $[b_v^2, b_\delta^{bc}] = [0.036, 1.5]$), where the last term in the square brackets includes the correlation between b_v^2 and b_δ^{bc} used for the combined fits in columns 8 and 9. These fits show no evidence for a significant detection of any of the relative velocity parameters.

	Fit to the data							
	$+\,b_v^2$		$+\,b_\delta^{bc}$		$+\,b_\theta^{bc}$		$+\,b_{v^2} + b_\delta^{bc}$	
	max. like.	mean	max. like.	mean	max. like.	mean	max. like.	mean
$\alpha_\perp$	1.000	1.002 ± 0.032	1.008	1.009 ± 0.029	1.007	1.012 ± 0.029	1.004	1.007 ± 0.030
$\alpha_\parallel$	0.999	1.004 ± 0.043	1.004	1.007 ± 0.040	1.003	1.007 ± 0.043	1.004	1.007 ± 0.039
$f\sigma_8$	0.480	0.481 ± 0.060	0.480	0.485 ± 0.062	0.476	0.477 ± 0.061	0.465	0.466 ± 0.063
$b_v^2[10^{-3}]$	14	$19 \pm 21(\pm 44)$	0	0	0	0	24	$24^{+18}_{-14}(^{+54}_{-34})$
b_δ	0	0	1.4	$1.4 \pm 4.3(^{+9.0}_{-12.0})$	0	0	6.2	$6.4 \pm 6.3(\pm 13.0)$
b_θ	0	0	0	0	−71	$-67 \pm 81(\pm 270)$	0	0
$b_1^{NGC}\sigma_8$	1.324	1.316 ± 0.047	1.346	1.348 ± 0.052	1.33	1.335 ± 0.052	1.358	1.351 ± 0.049
$b_1^{SGC}\sigma_8$	1.325	1.322 ± 0.058	1.340	1.340 ± 0.060	1.330	1.333 ± 0.060	1.371	1.362 ± 0.054
$b_2^{NGC}\sigma_8$	1.33	1.31 ± 0.76	1.20	1.32 ± 0.71	0.56	0.77 ± 0.76	1.58	1.28 ± 0.83
$b_2^{SGC}\sigma_8$	0.7	0.9 ± 1.0	0.52	0.67 ± 0.89	0.3	0.6 ± 1.0	1.24	1.22 ± 0.95
N^{NGC}	−1000	-300 ± 1700	−2600	-2700^{+1500}_{-1200}	−1100	-1600^{+2300}_{-1600}	−200	300^{+1500}_{-1200}
N^{SGC}	−1000	-600 ± 2000	−1700	-2100^{+2700}_{-1900}	−900	-1700^{+3500}_{-2300}	−900.0	-400 ± 1600
σ_v^{NGC}	5.85	5.79 ± 0.64	5.80	5.80 ± 0.66	5.63	5.63 ± 0.70	5.93	5.88 ± 0.69
σ_v^{SGC}	6.52	6.56 ± 0.85	6.44	6.50 ± 0.81	6.35	6.36 ± 0.81	6.70	6.66 ± 0.80
$\frac{\chi^2}{dof}$	$\frac{79.4}{74-12} = 1.28$ ($p = 0.067$)		$\frac{80.5}{74-12} = 1.30$ ($p = 0.057$)		$\frac{80.8}{74-12} = 1.30$ ($p = 0.055$)		$\frac{78.3}{74-13} = 1.28$ ($p = 0.067$)	

Table 3. Fits to the BOSS DR12 combined sample power spectrum multipoles in the high-redshift bin $0.5 < z < 0.75$. The fit includes the monopole and quadrupole in the range $0.01 < k < 0.15\,h^{-1}$ Mpc and the hexadecapole in the range $0.01 < k < 0.10\,h^{-1}$ Mpc. All errors in this table are the marginalised 68 per cent confidence levels, except of the error on the relative velocity parameters b_v^2, b_δ^{bc} and b_θ^{bc}, where we show both, the 68 per cent and 95 per cent confidence levels. We show fits including each relative velocity parameter in turn, meaning that columns 2 and 3 show the fits with b_v^2 as a free parameter assuming $b_\delta^{bc} = b_\theta^{bc} = 0$, etc. The relative velocity parameters are corrected by the bias we detected in the mock catalogues ($b_v^2 = 0.0265 \pm 0.0033$, $b_\delta^{bc} = -3.79 \pm 0.44$ and $b_\theta^{bc} = 187.2 \pm 4.7$, $[b_v^2, b_\delta^{bc}] = [0.036, 1.5]$), where the last term in the square brackets includes the correlation between b_v^2 and b_δ^{bc} used for the combined fits in columns 8 and 9. These fits show no evidence for a significant detection of any of the relative velocity parameters.

	Fit to the data							
	$+\,b_v^2$		$+\,b_\delta^{bc}$		$+\,b_\theta^{bc}$		$+\,b_{v^2} + b_\delta^{bc}$	
	max. like.	mean	max. like.	mean	max. like.	mean	max. like.	mean
$\alpha_\perp$	0.973	0.979 ± 0.028	0.971	0.975 ± 0.030	0.983	0.987 ± 0.026	0.972	0.976 ± 0.032
$\alpha_\parallel$	0.975	0.984 ± 0.043	0.980	0.987 ± 0.042	0.978	0.984 ± 0.043	0.980	0.985 ± 0.047
$f\sigma_8$	0.419	0.413 ± 0.047	0.416	0.409 ± 0.054	0.425	0.421 ± 0.048	0.420	0.417 ± 0.056
$b_v^2[10^{-3}]$	1	$4 \pm 21(\pm 43)$	0	0	0	0	−56	$-52 \pm 30(\pm 58)$
b_δ	0	0	−2.3	$-2.3 \pm 3.1(\pm 7.7)$	0	0	−10.4	$-10.8 \pm 3.6(\pm 8.9)$
b_θ	0	0	0	0	−152	$-155 \pm 76(\pm 230)$	0	0
$b_1^{NGC}\sigma_8$	1.219	1.232 ± 0.045	1.231	1.238 ± 0.046	1.163	1.162 ± 0.057	1.230	1.230 ± 0.060
$b_1^{SGC}\sigma_8$	1.239	1.243 ± 0.047	1.227	1.232 ± 0.050	1.262	1.261 ± 0.049	1.222	1.219 ± 0.055
$b_2^{NGC}\sigma_8$	2.94	$2.83^{+0.49}_{-0.61}$	0.72	$1.18^{+0.94}_{-1.20}$	−1.26	$-1.39^{+0.68}_{-0.55}$	0.66	0.77 ± 1.20
$b_2^{SGC}\sigma_8$	0.81	0.94 ± 0.79	0.74	0.85 ± 0.88	0.93	0.90 ± 0.93	0.68	0.68 ± 0.70
N^{NGC}	0	0 ± 1800	−1000	-1600^{+2400}_{-1100}	4700	5200 ± 2400	−1000	-1100 ± 2700
N^{SGC}	−500	-300 ± 1400	−1000	-1200^{+1700}_{-1200}	−1500	-1400^{+2000}_{-1400}	−1000	-700 ± 1600
σ_v^{NGC}	5.33	5.31 ± 0.75	5.11	5.10 ± 0.80	4.36	4.3 ± 1.0	5.06	5.02 ± 0.83
σ_v^{SGC}	4.94	4.94 ± 0.88	4.79	4.70 ± 0.91	4.99	4.86 ± 0.90	4.74	4.66 ± 0.97
$\frac{\chi^2}{dof}$	$\frac{51.7}{74-12} = 0.83$ ($p = 0.821$)		$\frac{55.3}{74-12} = 0.89$ ($p = 0.714$)		$\frac{52.0}{74-12} = 0.84$ ($p = 0.813$)		$\frac{55.2}{74-13} = 0.90$ ($p = 0.685$)	

the high-redshift bin is slightly below 1, while for the high-redshift bin, this quantity is slightly above 1, consistent with the findings of Beutler et al. (2016b). The p-values provided in brackets indicate that these deviations from unity are not significant.

Combining the high- and low-redshift bins, we find the following limits on the three relative velocity parameters: $b_v^2 = 0.012 \pm 0.015(\pm 0.031)$, $b_\delta^{bc} = -1.0 \pm 2.5(\pm 6.2)$ and $b_\theta^{bc} = -114 \pm 55(\pm 175)$ with 68 per cent (95 per cent) confidence levels.

If we treat the relative velocity effect as a pure suppression of star formation in regions where the relative velocity exceeds the virial velocity of haloes, we can apply a prior of $b_v^2 < 0$ (Dalal et al. 2010). This improves our constraints on b_v^2 to $|b_v^2| < 0.007 (< 0.018)$ (68 per cent and 95 per cent confidence levels).

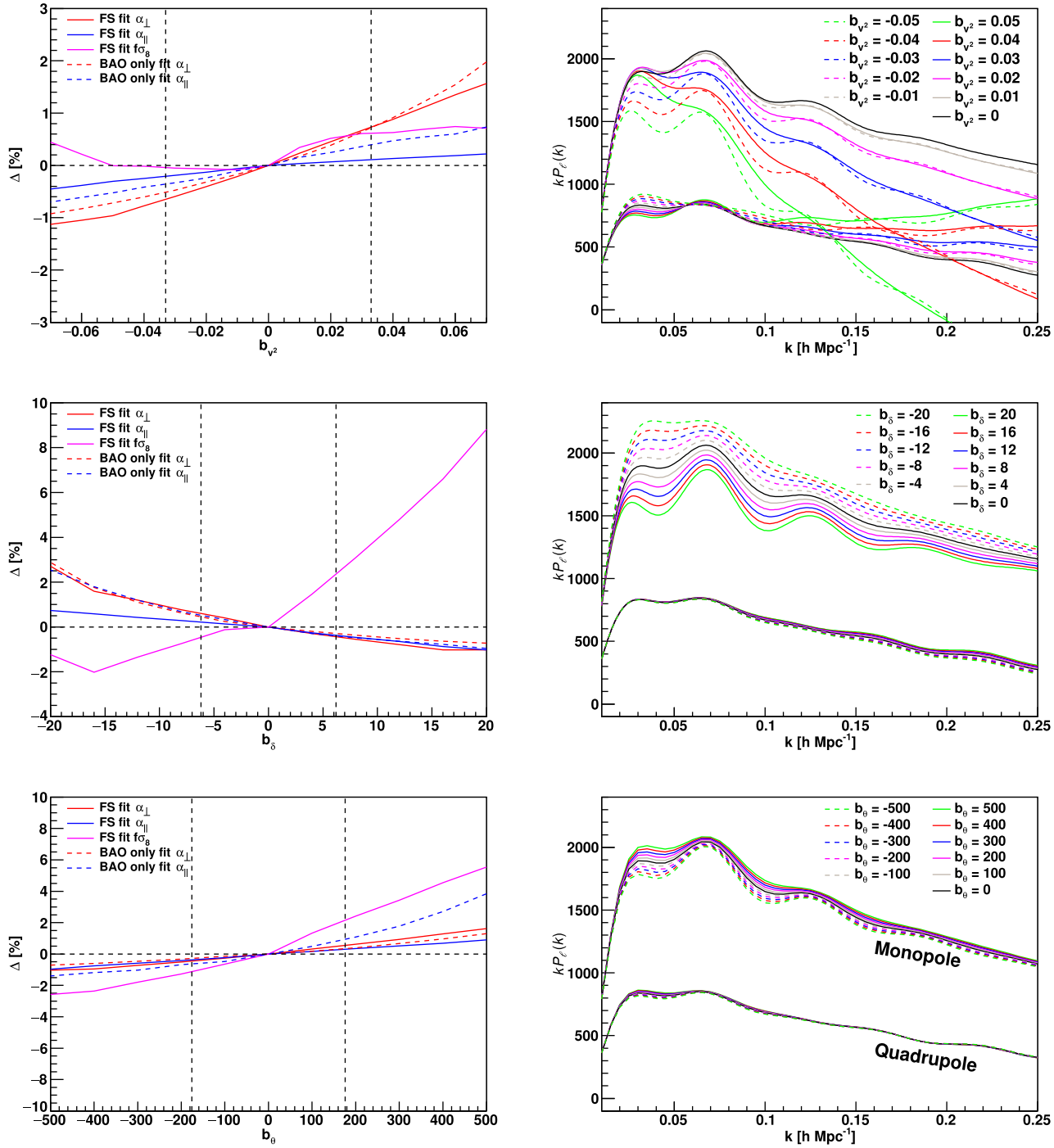

Figure 5. Here, we show the dependence of the shift parameters $\alpha_\perp$ and $\alpha_\parallel$ as well as the growth of structure parameter $f\sigma_8$ on the three relative velocity parameters (left-hand panel) and the change in the power spectrum model (right-hand panel). The solid lines in the plots on the left-hand side show the 'full shape' (FS) fits using the analysis pipeline of Beutler et al. (2016b), while the dashed lines use the BAO-only analysis pipeline of Beutler et al. (2016a). The vertical black dashed lines show the 95 per cent confidence levels for the three relative velocity parameters obtained in this paper (see Section 6).

7 QUANTIFYING THE POTENTIAL SYSTEMATIC UNCERTAINTIES FOR BAO AND RSD

Here, we want to quantify the potential bias for the anisotropic BAO parameters as well as the RSD parameter, depending on the amplitude of the three relative velocity parameters. To do this, we generate power spectrum models as shown in Section 4, and fit these models with the BAO-only fitting pipeline of Beutler et al. (2016a) and the 'full shape' pipeline of Beutler et al. (2016b). The results are shown in Fig. 5. The vertical black dashed lines show the 95 per cent confidence levels from our analysis.

All three relative velocity parameters are able to shift the BAO scale. The biases are quite different for the two BAO scaling parameters, $\alpha_\perp$ and $\alpha_\parallel$. The largest shift in $\alpha_\perp$ is due to b_v^2 and reaches 0.8 per cent at $b_v^2 = 0.031$ (which is the 95 per cent confidence limit

we found). The angular BAO scale $\alpha_\parallel$ shows 1 per cent shifts due to $b_\theta^{\rm bc}$.

We also include the shift in the RSD parameter $f\sigma_8$. Given that $b_\delta^{\rm bc}$ and $b_\theta^{\rm bc}$ mainly change the monopole to quadrupole ratio, we can see large effects on the RSD parameter of up to 2 per cent in both $b_\delta^{\rm bc}$ and $b_\theta^{\rm bc}$. Note that the latest measurement from the BOSS survey reported constraints of 1.5 per cent on $D_A(z)$, 2 per cent on $H(z)$ and 9 per cent on $f\sigma_8$.[2]

8 DISCUSSION

In Alam et al. (2016), the potential impact of the relative velocity effect on the BOSS-DR12 BAO measurement has been investigated using a configuration-space model following Blazek et al. (2015). The potential shift in the isotropic BAO scale (α) has been limited to 0.3σ, which is consistent with our results for b_{v^2}. The potential shifts by $b_\delta^{\rm bc}$ and $b_\theta^{\rm bc}$ have not been investigated.

Using the three-point correlation function, Slepian et al. (2016) constrain the relative velocity parameter b_{v^2} to $b_{v^2} < 0.0097$ (68 per cent confidence level). When using the 68 per cent confidence levels, we find $b_{v^2} = 0.012 \pm 0.015$ when combining the low- and high-redshift bins. When including the $b_{v^2} < 0$ prior, we get tighter constraints of $|b_{v^2}| < 0.007 (<0.018)$ (68 per cent and 95 per cent confidence levels). Slepian et al. (2016) do not investigate the linear bias parameters $b_\delta^{\rm bc}$ and $b_\theta^{\rm bc}$.

Yoo & Seljak (2013) used the power spectrum monopole to set the constraint $b_{v^2} < 0.033$ (95 per cent confidence level). However, there is a factor of 3 difference in the parametrization, which means that their constraint translates to $b_{v^2} < 0.1$ when using our nomenclature. This constraint is weaker by over one order of magnitude compared to our result. Part of the reason for our much tighter constraint is the increase in survey area between BOSS DR9 (used in Yoo & Seljak 2013) and BOSS DR12 (used in this work). Another reason for the improved constraints is the advection term, which is significantly contributing to our parameter constraint and which has not been included in the analysis of Yoo & Seljak (2013). Note that our results are not depending significantly on the inclusion of the quadrupole.

Yoo & Seljak (2013) also pointed out that the relative velocity effect might have an enhanced signature in the cross-correlation of two different galaxy samples. The idea is that one sample contains old galaxies, which formed early and retained the relative velocity effect, while the second sample contains young galaxies that will have a smaller (or no) relative velocity effect. Such an analysis was performed in Beutler et al. (2015) using the BOSS and WiggleZ galaxies. The BOSS sample contains mainly old LRG galaxies, which should carry a stronger relative velocity effect, compared to the ELG galaxies observed in WiggleZ. However, no relative velocity effect was detected and the best obtained constraint was $-0.086 < b_{v^2} < 0.062$ (68 per cent confidence level). These constraints use the same nomenclature as Yoo & Seljak (2013) and hence have to be multiplied by a factor of 3 before being compared to our constraints. Given that BOSS and WiggleZ overlap only in about 8 per cent of the total BOSS sky coverage, the cosmic volume available for this study was significantly smaller than BOSS alone. This analysis also did not include the advection term.

Finally, we note that our measurement of $b_1 \approx 2$ is in good agreement with other studies on the BOSS power spectrum (e.g. Gil-Marín et al. 2016), while Slepian et al. (2016) found a smaller value of $b_1 = 1.776 \pm 0.020$. The tension likely comes from the fact that the model of Slepian et al. (2016) did not include the tidal tensor bias, which can increase b_1 to 2.069 (Slepian et al. 2016), which is consistent with our measurement.

[2] Here, we quote the combined constraints from the two independent redshift bins.

9 CONCLUSION

We analysed the BOSS DR12 power spectrum multipoles using a power spectrum model for the relative velocity effect. We derive all redshift-space one-loop terms for the relative velocity, extending models used in previous analysis (see Appendix A). For the first time, we include the advection terms as suggested in Blazek et al. (2015). An analysis without the advection term is presented in Yoo & Seljak (2013). Besides the relative velocity parameter b_{v^2}, we also include the linear density and velocity divergence terms $b_\delta^{\rm bc}$ and $b_\theta^{\rm bc}$. Our main results can be summarized as follows:

(i) We extend the redshift-space clustering model of Beutler et al. (2014, 2016b) to include all relative velocity terms up to second order in b_{v^2} and linear order in $b_\delta^{\rm bc}$ and $b_\theta^{\rm bc}$.

(ii) Using two sets of N-body simulations and the BOSS DR12 Multidark-Patchy mock catalogues, we detect biases in the three relative velocity parameters of up to 2σ in $b_\theta^{\rm bc}$ and $\sim 1\sigma$ in b_{v^2} and $b_\delta^{\rm bc}$, indicating shortcomings of our power spectrum model. We correct the measurements by these biases but note that our model for the power spectrum does require further improvement. These biases should be kept in mind when using our constraints.

(iii) Our data does not support a detection of the relative velocity effect in any of the three relative velocity parameters. Combining the low- and high-redshift bins, we found limits of $b_{v^2} = 0.012 \pm 0.015 (\pm 0.031)$, $b_\delta^{\rm bc} = -1.0 \pm 2.5 (\pm 6.2)$ and $b_\theta^{\rm bc} = -114 \pm 55 (\pm 175)$ with 68 per cent (95 per cent) confidence levels. Including a prior of $b_{v^2} < 0$ motivated by treating the relative velocity effect as a pure suppression effect, our constraint on b_{v^2} tightens to $|b_{v^2}| < 0.018$ (95 per cent confidence levels).

(iv) Using the BOSS DR12 Fourier-space pipelines for BAO and RSD analysis, we quantify the potential systematic uncertainties in the BAO scale and RSD parameter due to the three relative velocity contributions. Our constraints limit the potential systematic shift in $D_A(z)$, $H(z)$ and $f\sigma_8$, due to the relative velocity effect to 1 per cent, 0.8 per cent and 2 per cent, respectively. Given the current uncertainties on the BAO measurements of BOSS, these shifts correspond to 0.53σ, 0.50σ and 0.22σ for $D_A(z)$, $H(z)$ and $f\sigma_8$, respectively.

In our analysis, we did not make use of density field reconstruction, which can significantly improve the BAO signal. Right now, we do not have a good model for the broad-band shape of the power spectrum post-reconstruction due to the complicated impact of the reconstruction procedure. We therefore leave such investigations for future work.

ACKNOWLEDGEMENTS

FB would like to thank Fabian Schmidt for help with the implementation of the $b_\delta^{\rm bc}$ and $b_\theta^{\rm bc}$ terms as well as valuable comments to this manuscript. FB would also like to thank Jonathan Blazek, Andreu Font-Ribera, Thomas Tram and Shun Saito for fruitful discussions. FB acknowledges support from the UK Space Agency through grant ST/N00180X/1. US is supported by NASA grant NNX15AL17G.

REFERENCES

Alam S. et al., 2016
Anderson L. et al., 2014, MNRAS, 441, 24
Baldauf T., Seljak U., Desjacques V., McDonald P., 2012
Barkana R., Loeb A., 2011, MNRAS, 415, 3113
Beutler F. et al., 2011, MNRAS, 416, 3017
Beutler F. et al., 2014, MNRAS, 443, 1065
Beutler F., Blake C., Koda J., Marin F., Seo H.-J., Cuesta A. J., Schneider D. P., 2015, MNRAS, 455, 3230
Beutler F. et al., 2016a
Beutler F. et al., 2016b
Bianchi D., Gil-Marín H., Ruggeri R., Percival W. J., 2015, MNRAS, 453, L11
Blake C., Glazebrook K., 2003, ApJ, 594, 665
Blake C. et al., 2011, MNRAS, 418, 1707
Blazek J., McEwen J. E., Hirata C. M., 2015
Bolton A. S. et al., 2012, AJ, 144, 144
Chan K. C., Scoccimarro R., Sheth R. K., 2012
Cole S. et al., 2005, MNRAS, 362, 505
Crocce M., Scoccimarro R., 2008, Phys. Rev. D, 77
Dalal N., Pen U.-L., Seljak U., 2010, J. Cosmol. Astropart. Phys., 2010, 007
Dawson K. S. et al., 2012, AJ, 145, 10
Desjacques V., Jeong D., Schmidt F., 2016
Doi M. et al., 2010, AJ, 139, 1628
Eisenstein D. J., Hu W., Tegmark M., 1998, ApJ, 504, L57
Eisenstein D. J. et al., 2005, ApJ, 633, 560
Eisenstein D. J. et al., 2011, AJ, 142, 72
Feldman H. A., Kaiser N., Peacock J. A., 1994, ApJ, 426, 23
Fialkov A., Barkana R., Visbal E., Tseliakhovich D., Hirata C. M., 2013, MNRAS, 432, 2909
Fukugita M., Ichikawa T., Gunn J. E., Doi M., Shimasaku K., Schneider D. P., 1996, AJ, 111, 1748
Gil-Marín H., Percival W. J., Verde L., Brownstein J. R., Chuang C.-H., Kitaura F.-S., Rodríguez-Torres S. A., Olmstead M. D., 2016, MNRAS
Gunn J., Carr M., Rockosi C., Sekiguchi M., 1998, AJ, 116, 3040
Gunn J. E. et al., 2006, AJ, 131, 2332
Hu W., Haiman Z., 2003, Phys. Rev. D, 68
Kitaura F.-S. et al., 2016, MNRAS, 456, 4156
Klypin A., Yepes G., Gottlober S., Prada F., Hess S., 2014
Laureijs R. et al., 2011
Lesgourgues J., 2011
Linder E. V., 2003, Phys. Rev. D, 68
McDonald P., Roy A., 2009, J. Cosmol. Astropart. Phys., 2009, 020
McDonald P., Roy A., 2009b, J. Cosmol. Astropart. Phys., 2009, 020
Naoz S., Yoshida N., Gnedin N. Y., 2012, ApJ, 763, 27
Okumura T., Hand N., Seljak U., Vlah Z., Desjacques V., 2015
Padmanabhan N., White M., Cohn J. D., 2009, Phys. Rev. D, 79
Percival W. J. et al., 2001, MNRAS, 327, 1297
Reid B. A., Seo H.-J., Leauthaud A., Tinker J. L., White M., 2014
Ross A. J. et al., 2012, MNRAS, 424, 564
Ross A. J. et al., 2016
Saito S., Baldauf T., Vlah Z., Seljak U., Okumura T., McDonald P., 2014, Phys. Rev. D, 90
Saito S., Baldauf T., Vlah Z., Seljak U., Okumura T., McDonald P., 2014b, Phys. Rev. D, 90
Schlegel D. J. et al., 2009
Schmidt F., 2016
Scoccimarro R., 2015, Phys. Rev. D, 92
Seo H.-J., Eisenstein D. J., 2003, ApJ, 598, 720
Slepian Z. et al., 2016
Smee S. et al., 2013, AJ, 146, 32
Smith J. A. et al., 2002, AJ, 123, 2121
Taruya A., Nishimichi T., Saito S., 2010, Phys. Rev. D, 82
Taruya A., Nishimichi T., Saito S., 2010b, Phys. Rev. D, 82
Tseliakhovich D., Hirata C., 2010, Phys. Rev. D, 82
Tseliakhovich D., Barkana R., Hirata C., 2011, MNRAS, 418, 906
Wilson M. J., Peacock J. A., Taylor A. N., de la Torre S., 2015
Yoo J., Seljak U., 2013
Yoo J., Dalal N., Seljak U., 2011, J. Cosmol. Astropart. Phys., 2011, 018

APPENDIX A: PERTURBATIVE TERMS FOR THE POWER SPECTRUM MODEL

Our power spectrum model is given by

$$\begin{aligned} P_{\rm g}(k,\mu) = \exp\left\{-(fk\mu\sigma_{\rm v})^2\right\} \Big[& P_{\rm g,NL}(k,\mu) + 2b_1 b_\delta^{\rm bc} P_{\delta\delta_{\rm bc}} \\ & + 2b_1 b_\theta^{\rm bc} P_{\delta\theta{\rm bc}} + b_1 b_{\rm v^2}\left[P_{\delta|{\rm v}^2}(k) + P_{{\rm adv}|\delta}(k)\right] \\ & + b_2 b_{\rm v^2} P_{\delta^2|{\rm v}^2}(k) + b_s b_{\rm v^2} P_{s^2|{\rm v}^2}(k) + b_{\rm v^2}^2 P_{{\rm v}^2|{\rm v}^2}(k) \\ & - 2f\mu^2[b_1 b_{\rm v^2} P_{\delta|{\rm v}^2 v_\parallel}(k) + b_{\rm v^2}(P_{{\rm v}^2|v_\parallel}(k) + P_{{\rm adv}|{\rm v}_\parallel}(k)) \\ & + b_1 b_{\rm v^2} P_{{\rm v}^2|\delta v_\parallel}(k)] \\ & + f^2\mu^2 b_{\rm v^2}\left[\mu^2 P_{v_\parallel|{\rm v}^2{\rm v}_\parallel}(k) - I_1(k) - \mu^2 I_2(k)\right]\Big]. \end{aligned} \tag{A1}$$

The non-linear power spectrum model, $P_{\rm NL}(k,\mu)$, is given by

$$\begin{aligned} P_{\rm g,NL}(k,\mu) = & P_{{\rm g},\delta|\delta}(k) + 2f\mu^2 P_{{\rm g},\delta|\theta}(k) + f^2\mu^4 P_{\theta|\theta}(k) \\ & + b_1^3 A(k,\mu,\beta) + b_1^4 B(k,\mu,\beta), \end{aligned} \tag{A2}$$

where

$$\begin{aligned} P_{{\rm g},\delta|\delta}(k) = & b_1^2 P_{\delta|\delta}(k) + b_2 b_1 P_{\delta|\delta^2}(k) + b_s b_1 P_{\delta|s^2}(k) \\ & + 2b_{3{\rm nl}} b_1 \sigma_3^2(k) P_{\rm m}^{\rm lin}(k) + b_2^2 P_{\delta^2|\delta^2}(k) + b_2 b_s P_{\delta^2|s^2}(k) \\ & + b_s^2 P_{s^2|s^2}(k) + N, \end{aligned} \tag{A3}$$

$$\begin{aligned} P_{{\rm g},\delta|\theta}(k) = & b_1 P_{\delta|\theta}(k) + b_2 P_{\theta|\delta^2}(k) + b_s P_{\theta|s^2}(k) \\ & + b_{3{\rm nl}}\sigma_3^2(k) P_{\rm m}^{\rm lin}(k). \end{aligned} \tag{A4}$$

The standard density and velocity terms are given by

$$P_{\delta|\delta^2}(k) = 2\int \frac{{\rm d}^3q}{(2\pi)^3} P_{\rm m}^{\rm lin}(q) P_{\rm m}^{\rm lin}(k-q) F_2(\boldsymbol{q}, \boldsymbol{k}-\boldsymbol{q}), \tag{A5}$$

$$P_{\theta|\delta^2}(k) = \int \frac{{\rm d}^3q}{(2\pi)^3} P_{\rm m}^{\rm lin}(q) P_{\rm m}^{\rm lin}(k-q) G_2(\boldsymbol{q}, \boldsymbol{k}-\boldsymbol{q}), \tag{A6}$$

$$P_{\delta|s^2}(k) = 2\int \frac{{\rm d}^3q}{(2\pi)^3} P_{\rm m}^{\rm lin}(q) P_{\rm m}^{\rm lin}(k-q) F_2(\boldsymbol{q}, \boldsymbol{k}-\boldsymbol{q}) S_2(\boldsymbol{q}, \boldsymbol{k}-\boldsymbol{q}) \tag{A7}$$

$$P_{\theta|s^2}(k) = \int \frac{{\rm d}^3q}{(2\pi)^3} P_{\rm m}^{\rm lin}(q) P_{\rm m}^{\rm lin}(k-q) G_2(\boldsymbol{q}, \boldsymbol{k}-\boldsymbol{q}) S_2(\boldsymbol{q}, \boldsymbol{k}-\boldsymbol{q}), \tag{A8}$$

$$P_{\delta^2|\delta^2}(k) = \frac{1}{2}\int \frac{{\rm d}^3q}{(2\pi)^3} P_{\rm m}^{\rm lin}(q)\left[P_{\rm m}^{\rm lin}(k-q) - P_{\rm m}^{\rm lin}(q)\right], \tag{A9}$$

$$\begin{aligned} P_{\delta^2|s^2}(k) = & -\int \frac{{\rm d}^3q}{(2\pi)^3} P_{\rm m}^{\rm lin}(q)\Big[\frac{2}{3} P_{\rm m}^{\rm lin}(q) - P_{\rm m}^{\rm lin}(k-q) S_2 \\ & \times(\boldsymbol{q}, \boldsymbol{k}-\boldsymbol{q})\Big], \end{aligned} \tag{A10}$$

$$P_{s^2|s^2}(k) = -\frac{1}{2}\int \frac{\mathrm{d}^3q}{(2\pi)^3} P_{\rm m}^{\rm lin}(q)\left[\frac{4}{9}P_{\rm m}^{\rm lin}(q) - P_{\rm m}^{\rm lin}(k-q)S_2 \times (\boldsymbol{q}, \boldsymbol{k}-\boldsymbol{q})^2\right], \tag{A11}$$

$$\sigma_3^2(k) = \frac{105}{16}\int \frac{\mathrm{d}^3q}{(2\pi)^3} P_{\rm m}^{\rm lin}(q)\left[D_2(-\boldsymbol{q}, \boldsymbol{k})S_2(\boldsymbol{q}, \boldsymbol{k}-\boldsymbol{q}) + \frac{8}{63}\right]. \tag{A12}$$

The additional relative velocity terms without redshift-space distortions are

$$P_{\mathrm{adv}|\delta}(k) = \frac{4}{3}T_{\rm v}(k)kP_{\rm m}^{\rm lin}(k)L_s, \tag{A13}$$

$$P_{\delta|\mathrm{v}^2}(k) = 4\int \frac{\mathrm{d}^3\boldsymbol{q}}{(2\pi)^3} P_{\rm m}^{\rm lin}(q)P_{\rm m}^{\rm lin}(k-q)F_2(\boldsymbol{q}, \boldsymbol{k}-\boldsymbol{q})G_u \times (\boldsymbol{q}, \boldsymbol{k}-\boldsymbol{q})\mu(\boldsymbol{q}, \boldsymbol{k}-\boldsymbol{q}), \tag{A14}$$

$$P_{\delta^2|\mathrm{v}^2}(k) = 2\int \frac{\mathrm{d}^3\boldsymbol{q}}{(2\pi)^3} P_{\rm m}^{\rm lin}(q)\left[P_{\rm m}^{\rm lin}(k-q)\mu(\boldsymbol{q}, \boldsymbol{k}-\boldsymbol{q}) \times G_u(\boldsymbol{q}, \boldsymbol{k}-\boldsymbol{q}) + P_{\rm m}^{\rm lin}(q)G_u(\boldsymbol{q}, \boldsymbol{q})\right], \tag{A15}$$

$$P_{s^2|\mathrm{v}^2}(k) = 2\int \frac{\mathrm{d}^3\boldsymbol{q}}{(2\pi)^3} P_{\rm m}^{\rm lin}(q)\left[P_{\rm m}^{\rm lin}(k-q)S_2(\boldsymbol{q}, \boldsymbol{k}-\boldsymbol{q}) \times \mu(\boldsymbol{q}, \boldsymbol{k}-\boldsymbol{q})G_u(\boldsymbol{q}, \boldsymbol{k}-\boldsymbol{q}) + \frac{2}{3}P_{\rm m}^{\rm lin}(q)G_u(\boldsymbol{q}, \boldsymbol{q})\right], \tag{A16}$$

$$P_{\mathrm{v}^2|\mathrm{v}^2}(k) = 2\int \frac{\mathrm{d}^3\boldsymbol{q}}{(2\pi)^3} P_{\rm m}^{\rm lin}(q)\left[P_{\rm m}^{\rm lin}(k-q)\mu^2(\boldsymbol{q}, \boldsymbol{k}-\boldsymbol{q}) \times G_u^2(\boldsymbol{q}, \boldsymbol{k}-\boldsymbol{q}) - P_{\rm m}^{\rm lin}(q)G_u^2(\boldsymbol{q}, \boldsymbol{q})\right], \tag{A17}$$

with $\mu(\boldsymbol{k}_1, \boldsymbol{k}_2) = \frac{\boldsymbol{k}_1\cdot\boldsymbol{k}_2}{k_1k_2}$ and

$$L_s = \int \frac{k\,\mathrm{d}k}{2\pi^2} T_{\rm v}(k)P_{\rm lin}(k). \tag{A18}$$

The relative velocity redshift-space distortion terms are

$$P_{\delta|\mathrm{v}^2\mathrm{v}_\parallel}(k) = \frac{2}{3}T_{\rm v}(k)kP_{\rm lin}(k)L_s = \frac{1}{2}P_{\mathrm{adv}|\delta}(k), \tag{A19}$$

$$P_{\mathrm{v}^2|v_\parallel}(k) = 2\int \frac{\mathrm{d}^3\boldsymbol{q}}{(2\pi)^3} \frac{k\mu - q}{\sqrt{k^2 - 2kq\mu + q^2}} P_{\rm lin}(q)P_{\rm lin}(k-q) \times G_2(\boldsymbol{q}, \boldsymbol{k}-\boldsymbol{q})G_u(\boldsymbol{q}, \boldsymbol{k}-\boldsymbol{q}), \tag{A20}$$

$$P_{\mathrm{adv}|v_\parallel}(k) = -\frac{2}{3}T_{\rm v}(k)kP_{\rm lin}(k)L_s = -\frac{1}{2}P_{\mathrm{adv}|\delta}(k) = -P_{\delta|\mathrm{v}^2\mathrm{v}_\parallel}(k), \tag{A21}$$

$$P_{\mathrm{v}^2|\delta v_\parallel}(k) = 2\int \frac{\mathrm{d}^3\boldsymbol{q}}{(2\pi)^3} \frac{k\mu(k\mu - q)}{q\sqrt{k^2 - 2kq\mu + q^2}} \times P_{\rm lin}(q)P_{\rm lin}(k-q)G_u(\boldsymbol{q}, \boldsymbol{k}-\boldsymbol{q}), \tag{A22}$$

$$P_{v_\parallel|\mathrm{v}^2\mathrm{v}_\parallel}(k) = -\frac{4}{3}T_{\rm v}(k)kP_{\rm lin}(k)L_s = -P_{\mathrm{adv}|\delta}(k), \tag{A23}$$

$$P_{\mathrm{v}^2|\mathrm{v}_\parallel^2}(k) = I_1(k) + \mu^2 I_2(k), \tag{A24}$$

with

$$I_1(k) = k^2\int \frac{\mathrm{d}^3\boldsymbol{q}}{(2\pi)^3} \frac{k^2(1-\mu^2)(q-k\mu)}{\left[k^2 - 2kq\mu + q^2\right]^{3/2}} \times G_u(\boldsymbol{q}, \boldsymbol{k}-\boldsymbol{q})P_{\rm lin}(q)P_{\rm lin}(k-q), \tag{A25}$$

$$I_2(k) = k^2\int \frac{d^3\boldsymbol{q}}{(2\pi)^3} \frac{k^2(2k^2\mu^2 - k(3\mu^3+\mu)q + (3\mu^2-1)q^2)}{q\left[k^2 - 2kq\mu + q^2\right]^{3/2}} \times G_u(\boldsymbol{q}, \boldsymbol{k}-\boldsymbol{q})P_{\rm lin}(q)P_{\rm lin}(k-q). \tag{A26}$$

The symmetrized second-order PT kernels F_2, G_2, S_2 and G_u are given by

$$F_2(\boldsymbol{k}_1, \boldsymbol{k}_2) = \frac{5}{7} + \frac{2}{7}\left(\frac{\boldsymbol{k}_1\cdot\boldsymbol{k}_2}{k_1k_2}\right)^2 + \frac{\boldsymbol{k}_1\cdot\boldsymbol{k}_2}{2}\left(\frac{1}{k_1^2} + \frac{1}{k_2^2}\right), \tag{A27}$$

$$G_2(\boldsymbol{k}_1, \boldsymbol{k}_2) = \frac{3}{7} + \frac{\boldsymbol{k}_1\cdot\boldsymbol{k}_2}{2}\left(\frac{1}{k_1^2} + \frac{1}{k_2^2}\right) + \frac{4}{7}\left(\frac{\boldsymbol{k}_1\cdot\boldsymbol{k}_2}{k_1k_2}\right)^2, \tag{A28}$$

$$S_2(\boldsymbol{k}_1, \boldsymbol{k}_2) = \left(\frac{\boldsymbol{k}_1\cdot\boldsymbol{k}_2}{k_1k_2}\right)^2 - \frac{1}{3}, \tag{A29}$$

$$D_2(\boldsymbol{k}_1, \boldsymbol{k}_2) = \frac{2}{7}\left[S_2(\boldsymbol{k}_1, \boldsymbol{k}_2) - \frac{2}{3}\right], \tag{A30}$$

$$G_u(\boldsymbol{k}_1, \boldsymbol{k}_2) = -T_{\rm v}(k_1)T_{\rm v}(k_2). \tag{A31}$$

APPENDIX B: TABLES WITH FITTING RESULTS

Table B1. Fitting results for the mean of the 20 runA simulations in redshift space. We show the results for the three individual relative velocity parameters and for varying all three parameters simultaneously. The covariance matrix is derived from the Multidark-Patchy mock catalogues scaled according to the volume. We show 68 per cent confidence levels for most parameters, but also include the 95 per cent confidence levels in parentheses for the relative velocity parameters.

	Test on mean of the 20 runA redshift-space mocks									
	No relative velocity		Only b_{v^2}		Only b_δ		Only b_θ		$b_{v^2}+b_\delta$	
	max. like.	mean	max. like.	mean	max. like.	mean	max. like.	mean	max. like.	mean
$\alpha_\perp$	1	1	1	1	1	1	1	1	1	1
$\alpha_\parallel$	1	1	1	1	1	1	1	1	1	1
$f\sigma_8$	0.455	0.455	0.455	0.455	0.455	0.455	0.455	0.455	0.455	0.455
$b_v[10^{-3}]$	0	0	21.9	$22.2 \pm 6.8(\pm 14)$	0	0	0	0	7	$16 \pm 21(\pm 44)$
b_δ	0	0	0	0	−3.6	$-3.5 \pm 1.1(\pm 2.1)$	0	0	−2.7	$-1.4 \pm 3.4(\pm 6.9)$
b_θ	0	0	0	0	0	0	142	$147 \pm 51(^{+170}_{-98})$	0	0
$b_1\sigma_8$	1.219	$1.220^{+0.013}_{-0.018}$	1.2198	$1.2230^{+0.0069}_{-0.0096}$	1.2213	1.2208 ± 0.0067	1.2173	$1.2178^{+0.0081}_{-0.011}$	1.2218	$1.2200^{+0.0083}_{-0.011}$
$b_2\sigma_8$	0.12	$0.32^{+0.70}_{-0.47}$	0.37	0.61 ± 0.49	0.68	0.71 ± 0.37	0.38	$0.48^{+0.46}_{-0.36}$	0.66	0.60 ± 0.60
N	274.0	-100 ± 1200	−80	-410^{+760}_{-580}	−1090	-1150 ± 730	−350	-550 ± 860	−940	-550^{+1500}_{-1000}
σ_v	−4.80	-4.85 ± 0.18	−4.83	$-4.90^{+0.15}_{-0.11}$	−4.82	-4.83 ± 0.11	−4.85	-4.87 ± 0.14	−4.84	-4.85 ± 0.16

Table B2. Same as Table B1 but for the 10 runPB simulations. We show 68 per cent confidence levels for most parameters, but also include the 95 per cent confidence levels in parenthesis for the relative velocity parameters.

	Test on mean of the 10 runPB redshift-space mocks									
	No relative velocity		Only b_{v^2}		Only b_δ		Only b_θ		$b_{v^2}+b_\delta$	
	max. like.	mean	max. like.	mean	max. like.	mean	max. like.	mean	max. like.	mean
$\alpha_\perp$	1	1	1	1	1	1	1	1	1	1
$\alpha_\parallel$	1	1	1	1	1	1	1	1	1	1
$f\sigma_8$	0.472	0.472	0.472	0.472	0.472	0.472	0.472	0.472	0.472	0.472
$b_v[10^{-3}]$	0	0	19	$20 \pm 11(\pm 21)$	0	0	0	0	48.8	$45 \pm 26(\pm 50)$
b_δ	0	0	0	0	−2.2	$-2.3 \pm 1.5(\pm 3.0)$	0	0	5.0	$4.2 \pm 4.1(\pm 8.1)$
b_θ	0	0	0	0	0	0	82	$77 \pm 63(\pm 120)$	0	0
$b_1\sigma_8$	1.268	$1.268^{+0.013}_{-0.016}$	1.268	1.2684 ± 0.0092	1.2683	$1.2684^{+0.0092}_{-0.012}$	1.267	$1.268^{+0.011}_{-0.014}$	1.262	1.266 ± 0.012
$b_2\sigma_8$	0.42	$0.54^{+0.59}_{-0.44}$	0.65	0.79 ± 0.48	0.72	0.79 ± 0.46	0.56	$0.70^{+0.57}_{-0.45}$	0.21	$0.50^{+0.76}_{-0.54}$
N	−500	-760 ± 1100	−690	-760 ± 730	−1200	-1360^{+1000}_{-810}	−820	-1120^{+1100}_{-880}	950	520 ± 1400
σ_v	−5.55	-5.57 ± 0.15	−5.57	-5.60 ± 0.12	−5.54	-5.55 ± 0.13	−5.57	-5.59 ± 0.14	−5.59	$-5.62^{+0.13}_{-0.17}$

Table B3. Fitting results for our relative velocity model using the low-redshift bin ($0.2 < z < 0.5$) of the Multidark-Patchy mock catalogues including the NGC window function. We show 68 per cent confidence levels for most parameters, but also include the 95 per cent confidence levels in parenthesis for the relative velocity parameters.

	Test on mean of the 2045 Multidark-Patchy mocks for the redshift range $0.2 < z < 0.5$.									
	No relative velocity		Only b_{v^2}		Only b_δ		Only b_θ		$b_{v^2} + b_\delta$	
	max. like.	mean	max. like.	mean	max. like.	mean	max. like.	mean	max. like.	mean
$\alpha_\perp$	1	1	1	1	1	1	1	1	1	1
$\alpha_\parallel$	1	1	1	1	1	1	1	1	1	1
$f\sigma_8$	0.484	0.484	0.484	0.484	0.484	0.484	0.484	0.484	0.484	0.484
$b_v[10^{-3}]$	0	0	29.1	$29.8 \pm 5.0(\pm 9.6)$	0	0	0	0	36	$34 \pm 12(\pm 22)$
b_δ	0	0	0	0	−4.96	$-4.78 \pm 0.78(\pm 1.6)$	0	0	1.2	$0.5 \pm 2.0(\pm 4.2)$
b_θ	0	0	0	0	0	0	187.2	$187.0 \pm 6.8(\pm 9.6)$	0	0
$b_1^{NGC}\sigma_8$	1.347	1.345 ± 0.010	1.3489	1.345 ± 0.010	1.3547	$1.3521^{+0.0076}_{-0.0095}$	1.348	1.344 ± 0.033	1.3392	1.3432 ± 0.0093
$b_1^{SGC}\sigma_8$	1.344	1.348 ± 0.016	1.3591	$1.359^{+0.011}_{-0.014}$	1.3585	$1.3600^{+0.0092}_{-0.013}$	1.343	1.348 ± 0.031	1.352	1.355 ± 0.012
$b_2^{NGC}\sigma_8$	0.17	0.15 ± 0.20	0.50	$0.58^{+0.30}_{-0.23}$	0.90	0.82 ± 0.26	0.46	0.5 ± 1.5	0.27	$0.44^{+0.45}_{-0.25}$
$b_2^{SGC}\sigma_8$	−0.01	0.08 ± 0.28	0.60	0.67 ± 0.38	0.80	0.89 ± 0.34	0.2	0.2 ± 1.3	0.41	$0.57^{+0.45}_{-0.33}$
N^{NGC}	−470	-420 ± 680	−980	-1040 ± 530	−2550	-2360 ± 600	−1340	-1330 ± 320	−260	-600 ± 840
N^{SGC}	210	-60 ± 980	−1150	-1190 ± 670	−2260	-2460^{+870}_{-660}	−510	-510 ± 330	−530	-930 ± 870
σ_v^{NGC}	5.89	5.87 ± 0.11	5.94	5.96 ± 0.11	5.94	5.91 ± 0.10	5.95	5.89 ± 0.66	5.91	$5.94^{+0.12}_{-0.09}$
σ_v^{SGC}	5.88	5.91 ± 0.14	6.06	6.08 ± 0.14	5.99	6.01 ± 0.13	5.92	5.97 ± 0.68	6.03	6.06 ± 0.14

Table B4. Fitting results for our relative velocity model using the high-redshift bin of the Multidark-Patchy mock catalogues including the NGC window function. We show 68 per cent confidence levels for most parameters, but also include the 95 per cent confidence levels in parenthesis for the relative velocity parameters.

	Test on mean of the 2045 Multidark-Patchy redshift-space mocks in the redshift range $0.5 < z < 0.75$									
	No relative velocity		Only b_{v^2}		Only b_δ		Only b_θ		$b_{v^2} + b_\delta$	
	max. like.	mean	max. like.	mean	max. like.	mean	max. like.	mean	max. like.	mean
$\alpha_\perp$	1	1	1	1	1	1	1	1	1	1
$\alpha_\parallel$	1	1	1	1	1	1	1	1	1	1
$f\sigma_8$	0.478	0.478	0.478	0.478	0.478	0.478	0.478	0.478	0.478	0.478
$b_v[10^{-3}]$	0	0	27.6	$27.0^{+6.2}_{-7.9}(^{+19}_{-22})$	0	0	0	0	40.3	$40.3 \pm 9.4(\pm 20)$
b_δ	0	0	0	0	−3.44	$-3.47 \pm 0.66(\pm 1.3)$	0	0	2.1	$2.0 \pm 1.4(^{+3.4}_{-2.6})$
b_θ	0	0	0	0	0	0	191.9	$192.5 \pm 6.5(\pm 9.4)$	0	0
$b_1^{NGC}\sigma_8$	1.3309	1.3320 ± 0.0087	1.3266	1.3272 ± 0.0064	1.3244	$1.3250^{+0.0058}_{-0.0075}$	1.324	1.326 ± 0.032	1.3255	1.3266 ± 0.0067
$b_1^{SGC}\sigma_8$	1.308	1.311 ± 0.012	1.3175	1.3169 ± 0.0066	1.3116	$1.3138^{+0.0078}_{-0.010}$	1.312	1.310 ± 0.036	1.3143	$1.3161^{+0.0080}_{-0.011}$
$b_2^{NGC}\sigma_8$	0.55	0.60 ± 0.29	0.83	0.85 ± 0.32	0.82	0.92 ± 0.25	0.8	1.0 ± 1.4	0.67	0.74 ± 0.33
$b_2^{SGC}\sigma_8$	0.19	$0.27^{+0.39}_{-0.29}$	0.86	$0.84^{+0.39}_{-0.28}$	0.70	0.85 ± 0.32	0.8	1.0 ± 1.3	0.59	0.68 ± 0.41
N^{NGC}	−999	-1110 ± 620	−943	-900 ± 350	−1570	-1710 ± 420	−1530	-1520 ± 330	−290	-360 ± 600
N^{SGC}	0	-200 ± 800	−873	-800 ± 320	−1220	-1430 ± 610	−1270	-1240 ± 310	−100	-170 ± 690
σ_v^{NGC}	5.750	5.760 ± 0.097	5.758	5.762 ± 0.085	5.678	5.697 ± 0.084	5.76	5.81 ± 0.69	5.777	5.788 ± 0.082
σ_v^{SGC}	5.69	5.71 ± 0.13	5.83	5.86 ± 0.10	5.71	5.73 ± 0.12	5.81	5.83 ± 0.65	5.82	5.842 ± 0.098

This paper has been typeset from a TEX/LATEX file prepared by the author.